ACS OMEGA

http://pubs.acs.org/journal/acsodf

Article

Molecular Adsorption of H_2 on Small Neutral Silver–Copper Bimetallic Nanoparticles: A Search for Novel Hydrogen Storage Materials

Sathya M. Perera, Samanthika R. Hettiarachchi, and Jinasena W. Hewage*

Cite This: *ACS Omega* 2022, 7, 2316–2330

Read Online

ACCESS | Metrics & More | Article Recommendations | Supporting Information

ABSTRACT: In the search for novel hydrogen storage materials, neutral silver–copper bimetallic nanoparticles up to the size of eight atoms (Cu_mAg_n: $m + n \leq 8$) have been computationally studied. Density functional theory with the B3LYP exchange–correlation functional and the combined basis sets of LanL2DZ and aug-cc-pVQZ were used in all of the calculations. H_2 adsorption studies on the most stable cluster geometries of all of the neat and heterogeneous entities found that 12 potential candidates, $CuAg_4$, Cu_6, Cu_5Ag, Cu_4Ag_2, Cu_3Ag_3, Cu_2Ag_4, $CuAg_6$, Cu_5Ag_3, Cu_4Ag_4, Cu_3Ag_5, Cu_2Ag_6, and $CuAg_7$, fall within the recommended physisorption range of −18 to −6 kJ mol^{-1}. A correlation in the behavior of binding energy, vibrational frequency, average bond distance, highest occupied molecular orbital–lowest unoccupied molecular orbital (HOMO–LUMO) gap, and chemical hardness with H_2 adsorption was observed. This analysis further revealed that the H_2 adsorption to the cluster was either a parallel or a perpendicular alignment. The analysis of the electron configuration of each atom in the cluster and the H_2 molecule and the charge transfer analysis of these 12 clusters also showed that the physisorption in the perpendicular mechanism is due to an induced dipole interaction, while that in the parallel mechanism is due to a weak ionic interaction. The clusters identified with perpendicular adsorption, $CuAg_4H_2$, Cu_6H_2, $Cu_3Ag_3H_2$, and $Cu_2Ag_4H_2$, polarized the H_2 molecule but had no charge transfer with the H_2 molecule and those identified with parallel adsorption, Cu_5AgH_2, $Cu_4Ag_2H_2$, $CuAg_6H_2$, $Cu_5Ag_3H_2$, $Cu_4Ag_4H_2$, $Cu_3Ag_5H_2$, $Cu_2Ag_6H_2$, and $CuAg_7H_2$, pulled the electrons from the H_2 molecule and had charge transfer with the H_2 molecule. The shapes of the frontier molecular orbital diagrams of the HOMO and LUMO also followed this observation.

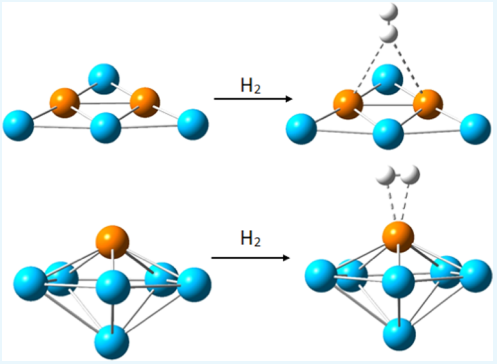

1. INTRODUCTION

Hydrogen is the most promising energy source as an environmentally friendly alternative to fossil fuels because it does not contribute to the carbon emission as fossil fuels when it is burnt, and it produces water. But the major problem is the storage of hydrogen to use it as an energy source. At the current state of technology, hydrogen must be compressed, liquefied, and stored in bulk tanks. In a bare system, because of its low boiling point (20.39 K), at least 1000 bar pressure is required to liquefy gaseous hydrogen at room temperature. Research on different chemical entities has been of growing interest in the search for novel storage materials. Metal–organic frameworks (MOFs), a class of highly porous crystalline materials, after the first promising results reported by the Yaghi group,[1,2] are being extensively studied.[3−9] The development of liquid hydrogen carriers such as liquid organic hydrogen carriers (LOHC) and ammonia is also considered to be a method of hydrogen storage, especially in renewable energy (wind, solar, etc.)-rich areas.[10−13] Different classes of metal–hydrogen complexes are being paid continuous attention in the search for potential storage materials.[14−23] Though there are several methods for hydrogen storage, other than compressing the gas, only that in which a material adsorbs hydrogen due to physisorption is a winning method to store hydrogen because of the absence of chemical bonds with the adsorbent and the reversibility of the process; hence, physisorption by porous solid-state materials and metal hybrids offers a solution to store hydrogen gas, but still, there are few materials that meet industrial requirements. Therefore, the search for hydrogen storage materials is a challenge in the early stage of the century for both experimentalists and theorists.

In parallel to experimental approaches, a considerable amount of theoretical work has been carried out in designing and characterizing storage materials. H_2 adsorption on a porous nanotube network,[24] as well as on oxygen-functionalized carbon slit pores,[25] was studied by the Froudakis group. They also reported the improved hydrogen storage abilities of

Received: November 2, 2021
Accepted: December 23, 2021
Published: January 7, 2022

Table 1. Comparison of the Calculated Binding Energies (BE/eV per Atom) and the Average First Neighbor Bond Distances ($\langle r\rangle$/Å) of Cu_n (n = 2−8) Clusters with Some of the Major Literature Data and Available Experimental Data[a]

		cohesive energy (BE)/eV per atom						average bond distance ($\langle r\rangle$)/Å			
cluster	PG symmetry and multiplicity	PW91[b]	TB-LMTO[c]	LSDA[d]	TBMD[e]	present	expt[e]	LSDA[d]	TBMD[e]	PW91[b]	present
Cu_2	$D_{\infty h}$ 1	1.055	0.23	1.36		1.01	1.02[f]	2.18		2.52	2.26
Cu_3	C_{2v} 2	1.187	0.68 (C_{3h})	1.52 (1.63)	1.43	1.00	1.07 ± 0.12	2.27	2.25	2.54	2.33
Cu_4	D_{2h} 1	1.580	1.28 (T_d)	1.97 (2.09)	2.00	1.31	1.48 ± 0.14	2.30	2.23	2.52	2.43
Cu_5	C_{2v} 2	1.724	1.43 (C_{4v})	2.01	2.24	1.41	1.56 ± 0.15	2.29	2.23	2.50	2.44
Cu_6	D_{3h} 1	1.909	1.56 (O_h)	− (2.49)	2.54 (C_{5v})	1.59	1.73 ± 0.18		2.40	2.47	2.44
Cu_7	D_{5h} 2	2.032	1.81(C_{2v})	−	2.63	1.63	1.86 ± 0.22		2.41	2.48	2.52
Cu_8	T_d 1	2.105	2.15 (D_{4d})	− (2.84)	2.87 (C_s)	1.73	2.00 ± 0.23		2.41	2.47	2.51

[a]Column 2 presents the point group symmetry of each species from the current study. Binding energies in parenthesis under the column LSDA are from ref 42. The experimental binding energy (1.02 eV per atom) is taken from ref 44. The calculated binding energies and the average bond distances in this study with the theory level of B3LYP/LanL2DZ are given in the columns "present". [b]Kuang et al.[39] [c]Lammers et al.[40] [d]Jackson and Massobrio et al.[41,42] [e]Kabir et al.[43] [f]Leopold et al.[44]

Li-doped metal−organic frameworks over undoped materials.[26] Humphries et al. reported the existence of transition-metal complex hydrides of which some are synthesized and characterized.[27] A comprehensive account of the current status of research on H_2 storage materials and applications has been documented by Hirscher et al.[28]

The possible use of transition-metal nanoclusters and their alloys as potential candidates for H_2 adsorption has been reported in the last two decades. In 2005, Guvelioglu reported the physicochemical properties of H_2-adsorbed small copper clusters.[29] Fang et al. studied H_2 adsorption on platinum-doped gold clusters.[30] A density functional study of molecular adsorption on small gold−copper binary clusters was also reported in 2015 by Zhao et al.[31] Very recently, Gálvez-González et al. reported H_2 adsorption on Au- and Pt-doped copper clusters with the size of four atoms.[32] The research focusing on the potential use of mixed transition-metal nanostructured materials for hydrogen storage is limited, and this study aims to explore a copper−silver mixed system in all compositions (Cu_mAg_n for $m + n \leq 8$) to find the most potential heterogeneous system within the recommended physisorption limit.

2. CALCULATION DETAILS

We used Kohn−Sham density functional theory (DFT) in all of the calculations of the bare cluster and H_2 adsorption using the Gaussian 16 software package.[33] In this study, we used the Becke 3 parameter Lee−Yang−Parr (B3LYP) correlation functional and the Los Alamos relativistic effective core potential for core electrons with double-ζ basis set for valence electrons (LanL2DZ) for Cu and Ag of the Cu_mAg_n system.[34] In the case of H_2 adsorption, we mixed the LanL2DZ basis set with Dunning's correlation-consistent basis set, aug-cc-pVQZ, for Cu and Ag, and H_2 of the $Cu_mAg_nH_2$ system, respectively. We will compare our results with the literature and rationalize the selection of the functional and basis set in Section 3.1.

3. RESULTS AND DISCUSSION

All of the possible geometries of Cu_mAg_n ($m + n \leq 8$) clusters were designed, and their global minimum was located by applying extensive optimization procedures at different special arrangements of copper and silver atoms including all possible spin arrangements and by the absence of the imaginary modes in the calculated Hessian. Then, the most stable neutral cluster species in each series of different cluster sizes were subjected to H_2 molecule adsorption. The H_2 adsorption on all of the different positions for each cluster was studied. The stability of the cluster series was compared utilizing the average binding energy (BE), adiabatic ionization and electron affinity, chemical hardness, and highest occupied molecular orbital−lowest unoccupied molecular orbital (HOMO−LUMO) gap (HLG). The hydrogen adsorption was characterized using similar parameters, such as hydrogen adsorption energy, bond distance analysis, vibrational frequency analysis, orbital occupancy analysis, and frontier molecular orbital (FMO) analysis.

The average binding energies of a Cu_mAg_n cluster and those of a hydrogen-adsorbed cluster are calculated as follows

$$\mathrm{ABE}(Cu_mAg_n) = [mE(Cu) + nE(Ag) - E(Cu_mAg_n)]/(m + n) \quad (1)$$

$$\mathrm{ABE}(Cu_mAg_nH_2) = [mE(Cu) + nE(Ag) + 2E(H) - E(Cu_mAg_nH_2)]/(m + n + 2) \quad (2)$$

Adiabatic ionization potential (AIP) and adiabatic electron affinity (AEA) of both Cu_mAg_n and $Cu_mAg_nH_2$ clusters are calculated using the following expressions

$$\mathrm{AIP}(Cu_mAg_n) = E(Cu_mAg_n)^+ - E(Cu_mAg_n) \quad (3)$$

$$\mathrm{AEA}(Cu_mAg_n) = E(Cu_mAg_n) - E(Cu_mAg_n)^- \quad (4)$$

$$\mathrm{AIP}(Cu_mAg_nH_2) = E(Cu_mAg_nH_2)^+ - E(Cu_mAg_nH_2) \quad (5)$$

$$\mathrm{AEA}(Cu_mAg_nH_2) = E(Cu_mAg_nH_2) - E(Cu_mAg_nH_2)^- \quad (6)$$

In addition, chemical hardness (η), which is also a measure of the relative stability of an electronic system, can be estimated as half the difference between the adiabatic ionization potential and adiabatic electron affinity through the electronic chemical potential of the system.[35−38]

$$\eta = \frac{(\mathrm{AIP} - \mathrm{AEA})}{2} \quad (7)$$

The hydrogen adsorption energy is given by the equation

$$E_{\mathrm{Ad}} = E(Cu_mAg_n) + E(H_2) - E(Cu_mAg_nH_2) \quad (8)$$

https://doi.org/10.1021/acsomega.1c06146
ACS Omega 2022, 7, 2316−2330

Table 2. Comparison of Calculated Binding Energies (BE/eV per Atom) and the Average First Neighbor Bond Distances ($\langle r \rangle$/Å) of Ag_n (n = 2−8) Clusters[a]

		cohesive energy (BE)/eV per atom								average bond distance ($\langle r \rangle$)/Å	
cluster	PG symmetry and multiplicity	BP86[b]	revPBE[b]	B3LYP[b]	BPW91[c]	B2LYP[c]	PB86[c]	present	expt	present	expt
Ag_2	$D_{\infty h}$ 1	0.83	0.76	0.75	1.01	0.92	1.10	0.78	0.83[d]	2.61	2.48[f] (2.53)[g]
Ag_3	C_{2v} 2	0.82	0.74	0.71	0.99	0.88	1.09	0.74	0.87[e]	2.69	
Ag_4	D_{2h} 1	1.09	0.96	0.93				0.95		2.78	
Ag_5	C_{2v} 2	1.19	1.05	1.02				1.04		2.80	
Ag_6	D_{3h} 1	1.36	1.20	1.18				1.20		2.80	
Ag_7	D_{5h} 2	1.37	1.19	1.14				1.17		2.87	
Ag_8	T_d 1	1.46	2.28	1.28				1.26		2.87	

[a]Column 2 presents the point group symmetry of each species with the spin multiplicity in this study. Calculated binding energies under the functionals of BP86, revPBE, and B3LYP are from ref 45, those corresponding to the BPW91, B3LYP, and PB86 are from ref 47, and experimental values are from refs 46 and 48−50. The calculated binding energies and the average bond distances in this study with the theory level of B3LYP/LanL2DZ are given in the columns "present". [b]Liao et al.[45] [c]Srinivas et al.[47] [d]Beutel et al.[46] [e]Hilpert et al.[50] [f]Morse et al.[48] [g]Simard et al.[49]

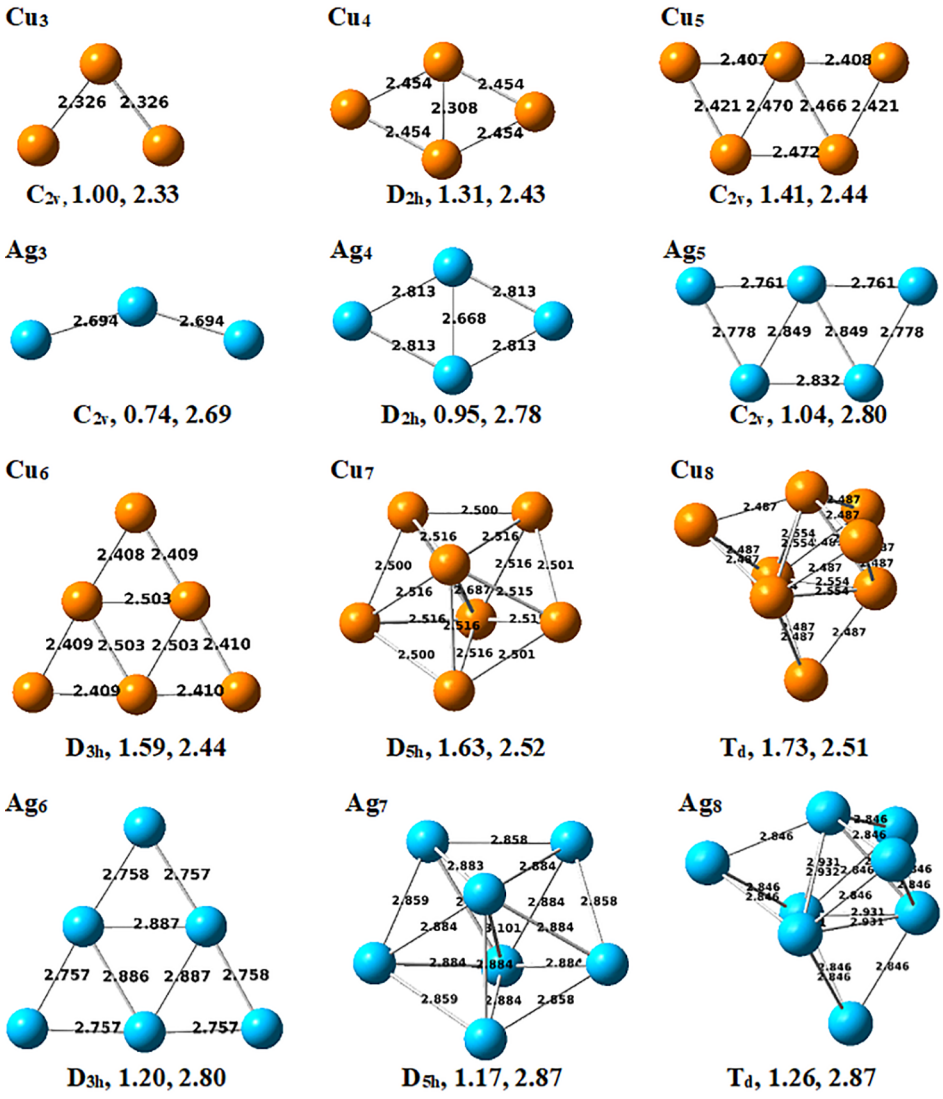

Figure 1. Lowest energy structures of Cu_n (orange) and Ag_n (blue) clusters from n = 3 to 8. The values given below each cluster structure are in order of point group symmetry, binding energy (BE) in eV, and average bond distance of the cluster ($\langle r \rangle$) in Å. The equilibrium bond distances of Cu and Ag dimers are 2.259 and 2.611 Å, respectively.

3.1. Structures and Relative Stability of Bare Cu_mAg_n Clusters. The binding energies and spatial arrangements of atoms (point group symmetry) in the optimized structures with spin multiplicity given in Table 1 are compared with data of previous studies on Cu clusters obtained by different techniques, especially in generalized gradient approximation

https://doi.org/10.1021/acsomega.1c06146
ACS Omega 2022, 7, 2316−2330

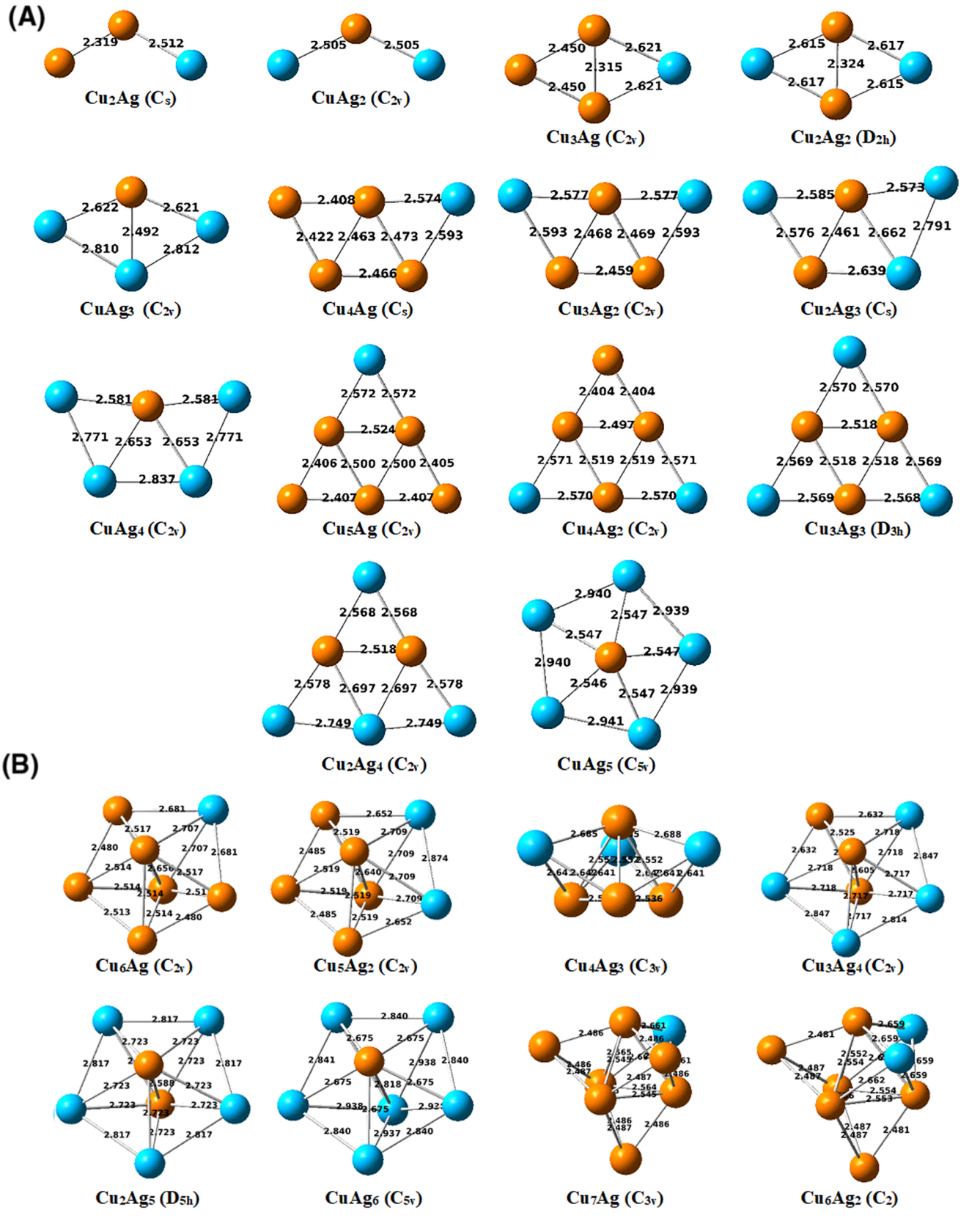

Figure 2. continued

https://doi.org/10.1021/acsomega.1c06146
ACS Omega 2022, 7, 2316−2330

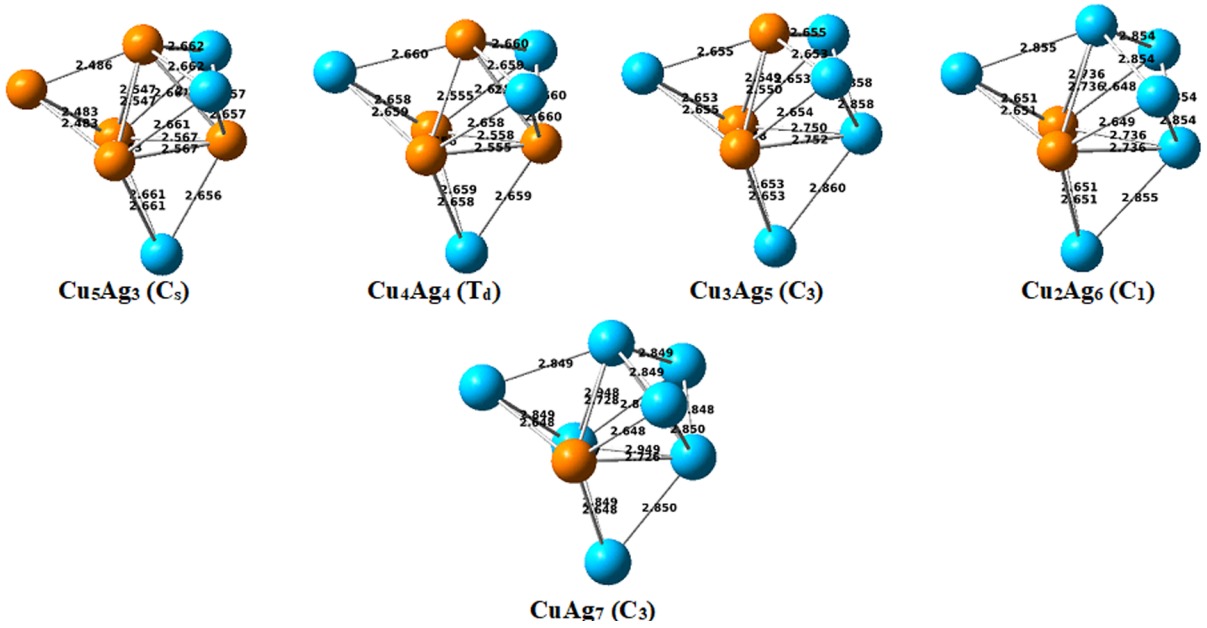

Figure 2. Lowest energy structures of Cu_mAg_n clusters from (a) $m + n = 3$ to 6. Tables 3 and 4 (b) $m + n = 7$ and 8. The point group symmetry of the cluster is given in parentheses. Orange and blue colors represent Cu and Ag atoms, respectively. The binding energy (BE) in eV and average bond distance of the cluster ($\langle r \rangle$) in Å with other physical parameters are given in Tables 3 and 4, respectively.

(GGA) at the PW91 level, parameterized tight-binding linear muffin-tin orbital (TB-LMTO), local-spin-density approximation (LSDA), and tight-binding molecular dynamics (TBMD) with parameters fitted to first-principles calculations by Kuang et al.,[39] Lammers et al.,[40] Jackson and Massobrio et al.,[41,42] and Kabir et al.,[43] respectively. The binding energies derived from both the local-spin-density approximation and from the tight-binding molecular dynamics showed overestimated figures compared to the experimental values and those derived from generalized gradient approximation were relatively in agreement with the experimental values. Similarly, the binding energies calculated using the parameterized tight-binding linear muffin-tin orbital were also in good agreement with the experimental values for the clusters larger than $n = 3$ though cluster symmetries were inconsistent. The calculated values in this study using DFT with the B3LYP correlation functional and the basis set of LanL2DZ showed excellent agreement with experimental values. In the case of the dimer, the calculated binding energy (1.01 eV per atom) and the bond distance (2.26 Å) showed excellent agreement with those of experimental values (1.02 eV per atom and 2.22 Å, respectively).[44]

Similarly, Table 2 compares the binding energies of neat Ag clusters reported in two different studies and obtained in the present study with the available experimental data of the Ag dimer and trimer. Liao et al.[45] compared the binding energies per atom of the Ag clusters calculated by three density functionals, generalized gradient approximation (GGA) at BP86 and revPBE, and B3LYP with the experimental binding energy of the Ag dimer.[46] In this comparison, STO basis functions with triple zeta frozen core plus 1 polarization function (TZP fc) were used and BP86 was considered as the best suit on their study of oxygen adsorption on both neutral and anionic silver and gold clusters. On the other hand, Srinivas et al.[47] reported the performance of three DFT functionals, BPW91, B3LYP, and BP86, separately against two different 28-electron ECPs and an all-electron basis for the atomic orbital treatments by calculating and comparing the binding energy per atom of the dimer and trimer with those of experimental data.[48−50] Their study concluded that the performance depends on the choice of the specific functional within DFT and the basis set used in combination; in general, B3LYP showed better agreement with the binding energy. With these extensive comparisons, we selected the B3LYP/LanL2DZ combination for the calculation in our study, especially considering the copper clusters.

Minimum energy structures of both neat copper and silver motifs are shown in Figure 1. The dimension transitions (from 1-D to 3-D) of both copper and silver cluster structures occur when the cluster size increases. The dimer is a 1-D structure, the trimer to the hexamer possess planar 2-D structure patterns, and the clusters above the hexamer are in 3-D arrangements aligning with previous observations.[43,51] The clusters of both pure Cu_n and Ag_n have the shapes of an isosceles triangle for the trimer, rhombus for the tetramer, trapezoid for the pentamer, triangle for the hexamer, pentagonal bipyramid for the heptamer, and tetracapped tetrahedron for the octamer.

Both Cu and Ag belong to the coinage group (group 11) in the periodic table. The optimized structures of the mixed clusters given in Figure 2a,b show that the copper atoms always tend to occupy the middle position when it is available due to the smaller size of the Cu atom ($3d^{10}4s^1$) compared to the Ag atom ($4d^{10}5s^1$) and reduced electronegativity of Cu (1.9) compared to that of Ag (1.93) according to the general fact that atoms with the most positive charges favor the middle positions (nuclei) of the clusters, where an atom can have the optimal coordination number. The mixed clusters of each stoichiometric ratio of copper and silver were designed using the stable configurations of Cu_n clusters as the precursors. In this process, Cu atoms were systematically replaced by Ag atoms one by one accounting for all of the possible positions, and the most stable structure of each mixed cluster was obtained by energy optimization. The deviation from the

https://doi.org/10.1021/acsomega.1c06146
ACS Omega 2022, 7, 2316−2330

original monometallic cluster morphology with heterogeneity is also noticed. Different structural shapes for the different stoichiometry of copper and silver in a particular cluster size can be observed, and Cu atoms reside in such a way that they can possess the optimal coordination number. As shown in Figure 2a, the mixed clusters follow similar structural patterns of Ag_n and Cu_n clusters observed in this study as well as in previous work.[29,31,32,52] The dimer of the Cu_mAg_n cluster is a 1-D structure, whereas the trimer to the hexamer of Cu_mAg_n clusters possess planar 2-D structure patterns except for the 3-D structure of $CuAg_5$. Cu_mAg_n clusters above the hexamer are in 3-D arrangements (Figure 2b). The hexamers consist of triangular and capped spatial arrangements lying in a broad energy spectrum instead of pursuing the original triangular shape of Cu_6 and Ag_6. In contrast to the low symmetric (C_{2v}) triangular structure of $CuAg_5$ observed by Wei-Yin et al. (with four coordinated Cu),[51] we observed high symmetric (C_{5v}) capped spatial arrangements of the atoms with the maximum of five coordination for Cu following the observation made by Zhou and co-workers.[53] Though the $CuAg_5$ cluster possesses a capped shape, all of the other candidates in the hexamer are triangular including the Cu_5Ag cluster, whose single Ag atom is not favorable to be in the middle forming a capped shape structure because of comparatively high positive charge and small size of the Cu atom compared to Ag. All of the heptamers, except Cu_4Ag_3, possess the original pentagonal bipyramid structural shape of Cu_7 and Ag_7. Cu_4Ag_3 is a tricapped tetrahedron with the C_{3v} symmetry that consists of three layers of packing. The first layer is an equilateral triangle of three Cu atoms, the next layer is an equilateral triangle of three Ag atoms, and then the fourth Cu atom is above the center of the triangles. The minimum energy structures of single Cu atom-substituted cluster series, Ag_nCu, for n = 1−8, reported by Ding et al. using the meta-GGA functional were in accordance exactly with the structures observed in this study for the corresponding entities.[54]

In addition to these minimum energy structures, we examined the other higher energy structures (low-lying isomers) of Cu_mAg_n clusters for $m + n$ = 3−8, and the structures of those isomers with energies relative to the lowest energy geometry are given in Figure S2a−f in the Supporting Information. A detailed comparison of low-lying energy structures is beyond the scope of this article and interested readers can find a detailed comparison in the literature.[32,52−55]

The average bond distance of a cluster is also an important parameter to understand the cohesiveness of the cluster with its size. Figure 3 depicts the change of the average bond distances of Cu_n and Ag_n clusters with the number of atoms in the cluster. In addition, the variation of the average first neighbor bond distance of the $Cu_{(8-n)}Ag_n$ cluster for n = 1−7 with the silver substitution is also shown in the same graph. This shows that the cluster expansion with the consecutive addition of an atom to both neat copper and silver systems shows a uniform parallel behavior keeping the difference between the two at about 0.36 Å, which is approximately the difference of the equilibrium bond distances of the Ag dimer (2.61 Å) and the Cu dimer (2.26 Å). This reveals that the atomic radii (size of the atoms) play a major role in the cluster size expansion but not the electronic structure due to the same valence electronic configuration of Cu and Ag ($3d^{10}4s^1$ and $4d^{10}5s^1$, respectively). Similarly, the stepwise replacement of a copper atom in a cluster, $Cu_{(8-n)}Ag_n$, for example, by a silver atom shows a gradual increase of the average bond distance,

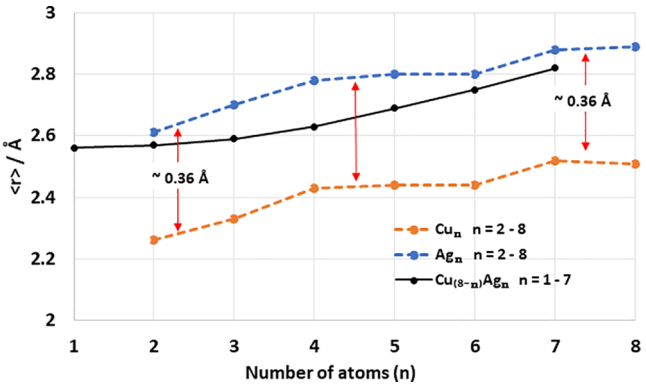

Figure 3. Variation in the average bond distance of neat copper clusters (Cu_n: orange) and silver clusters (Ag_n: blue) with the number of atoms in the cluster from n = 2 to 8. The black color plot shows the expansion of the $Cu_{(8-n)}Ag_n$ cluster with the substitution of a Ag atom in place of the Cu atom.

resulting in the expansion of the cluster size with the same number of atoms. In contrast to this gradual increase of the average bond distance for n = 1−7, as shown in Table 4, the abrupt change of the average bond distances occurs in the transition from Cu_8 to Cu_7Ag (from n = 0 to 1) and from $CuAg_7$ to Ag_8 (from n = 7 to 8). In the first case, the addition of a Ag atom to high symmetric Cu_8 causes symmetry loss from T_d to C_{3v} (Figures 1 and 2a,b), which increases the average bond distance compared to the addition of a Ag atom to the already symmetry lost clusters for $n \geq 1$. In the second case, the relaxation of low symmetric $CuAg_7$ occurs when the Ag atom is added to gain the high symmetry from C_3 to T_d.

Similarly, we can observe a rapid increase in the binding energy per atom compared to the slower rate of cluster expansion with the number of atoms in the cluster except for the slight decrease for n = 3 and 7 as shown in Figure 4.

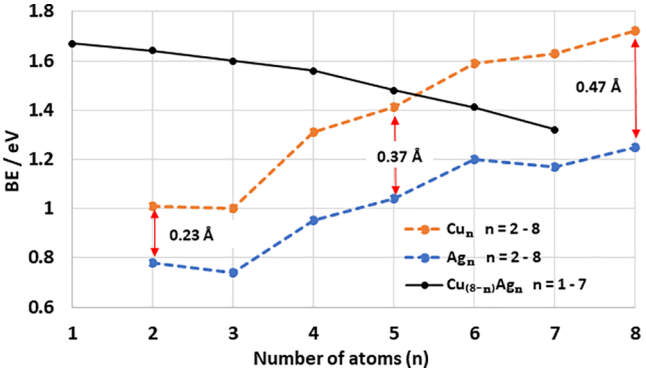

Figure 4. Variation in the binding energy of neat copper clusters (Cu_n: orange) and silver clusters (Ag_n: blue) with the number of atoms in the cluster from n = 2 to 8. The black color solid line shows the binding energy lowering of the $Cu_{(8-n)}Ag_n$ cluster with the substitution of a Ag atom in place of the Cu atom.

Interestingly, n = 3 and 7 are the points where we observed the dimensional transition from 1-D to 2-D and from 2-D to 3-D, respectively. Cu_n clusters have higher binding energies than corresponding Ag_n clusters and the energy gap (difference) increases with the number of atoms in the cluster; at the lower end, it accounts for 0.23 Å, which is the difference in two dimers, while at the higher end, it is about 0.47 Å. The cluster expansion and binding energy lowering with the replacement

https://doi.org/10.1021/acsomega.1c06146
ACS Omega 2022, 7, 2316−2330

Table 3. Comparison of Calculated Binding Energies (BE/eV per Atom) of Both Bare and H_2-Adsorbed clusters, H_2 Adsorption Energy of Cu_mAg_n ($m + n = 2-8$) Clusters, Adiabatic Ionization Potential, and Electron Affinity with Adiabatic Chemical Hardness, and Vertical Ionization Potential and Electron Affinity with Vertical Chemical Hardness of Bare and H_2-Aadsorbed Clusters[a]

Cluster	BE(eV)		E_{ads} (kJ mol^{-1})	HLG (eV)			AIP (eV)		AEA (eV)		η_a (eV)		VIP (eV)		VEA (eV)		η_v (eV)	
	bare	H_2 ads		bare	H_2 ads	Δ	bare	H_2 ads	bare	H_2 ads	bare	H_2 ads	bare	H_2 ads	bare	H_2 ads	bare	H_2 ads
Cu_2	1.01	1.78	-30.37	3.25	3.89	0.64	7.93	8.04	0.67	0.35	3.63	3.84	8.01	7.62	0.63	-0.17	3.69	3.90
CuAg	0.89	1.72	-29.42	3.08	3.72	0.64	7.83	7.93	0.83	0.69	3.50	3.62	7.89	7.54	0.78	-0.05	3.56	3.79
Ag_2	0.78	1.59	-3.19	2.91	3.10	0.19	7.73	7.71	0.99	1.01	3.37	3.35	7.80	7.62	0.93	0.63	3.43	3.50
Cu_3	1.00	1.67	-54.92	1.40	1.42	0.02	5.74	5.71	1.91	1.55	1.92	2.08	5.94	5.81	0.98	0.96	2.48	2.43
Cu_2Ag	0.93	1.62	-50.11	1.34	1.36	0.02	5.79	5.73	2.06	1.71	1.87	2.01	6.64	5.85	1.73	1.07	2.45	2.39
$CuAg_2$	0.86	1.56	-40.53	1.28	1.30	0.02	5.88	5.76	2.15	1.81	1.86	1.97	6.70	5.88	1.90	1.18	2.40	2.35
Ag_3	0.74	1.41	-5.91	1.26	1.28	0.02	5.80	5.61	2.22	2.20	1.79	1.71	6.85	5.75	2.13	1.14	2.36	2.31
Cu_4	1.31	1.78	-66.60	1.91	2.85	0.94	6.59	6.65	1.34	0.69	2.63	2.98	6.60	6.68	1.27	0.53	2.66	3.08
Cu_3Ag	1.24	1.74	-63.05	1.92	2.84	0.92	6.58	6.63	1.36	0.72	2.61	2.95	6.60	6.67	1.29	0.58	2.65	3.04
Cu_2Ag_2	1.18	1.69	-59.05	1.96	2.83	0.87	6.58	6.62	1.37	0.76	2.61	2.93	6.58	6.65	1.37	0.64	2.61	3.01
$CuAg_3$	1.07	1.60	-56.02	1.76	2.55	0.79	6.50	6.55	1.51	0.97	2.49	2.79	6.51	6.58	1.44	0.84	2.53	2.87
Ag_4	0.95	1.47	-19.31	1.61	2.22	0.61	6.42	6.39	1.62	1.49	2.40	2.45	6.43	6.41	1.54	0.98	2.45	2.71
Cu_5	1.41	1.73	-26.40	1.34	1.37	0.03	5.99	5.70	1.75	1.59	2.12	2.05	6.24	5.99	1.70	1.47	2.27	2.26
Cu_4Ag	1.35	1.69	-27.61	1.32	1.31	-0.01	6.02	5.75	1.82	1.69	2.10	2.03	6.24	6.00	1.77	1.58	2.24	2.21
Cu_3Ag2	1.29	1.65	-25.39	1.29	1.30	0.01	6.05	5.79	1.89	1.75	2.01	2.02	6.24	6.02	1.83	1.63	2.20	2.19
Cu_2Ag_3	1.22	1.59	-24.67	1.24	1.27	0.03	5.99	5.72	1.95	1.87	2.02	1.92	6.22	6.00	1.88	1.66	2.17	2.17
$CuAg_4$	1.14	1.51	**-8.55**	1.20	1.20	0	5.92	5.77	1.99	2.01	1.96	1.88	6.19	6.18	1.93	1.85	2.13	2.16
Ag_5	1.04	1.43	-5.13	1.18	1.18	0	5.82	5.83	2.00	2.03	1.91	1.90	6.15	6.15	1.94	1.96	2.10	2.09
Cu_6	1.59	1.81	**-16.71**	3.24	3.24	0	7.11	6.25	1.01	1.06	3.05	2.59	7.17	7.17	0.96	1.02	3.10	3.08
Cu_5Ag	1.54	1.78	**-15.89**	3.14	3.20	0.06	7.12	6.29	1.01	0.96	3.00	2.67	7.18	6.86	1.05	0.74	3.07	3.06
Cu_4Ag_2	1.49	1.74	**-15.45**	3.06	3.15	0.09	7.04	6.77	1.18	0.97	2.93	2.90	7.09	6.85	1.12	0.81	2.99	3.02
Cu_3Ag_3	1.44	1.70	**-12.89**	3.01	3.00	-0.01	7.04	6.41	1.26	1.29	2.89	2.56	7.10	7.10	1.20	1.24	2.95	2.93
Cu_2Ag_4	1.36	1.63	**-10.41**	2.98	2.98	0	7.00	6.30	1.27	1.30	2.86	2.50	7.06	7.06	1.21	1.24	2.93	2.91
$CuAg_5$	1.28	1.59	-22.70	2.98	3.01	0.03	6.68	6.48	1.21	1.08	2.73	2.70	6.91	6.83	1.01	0.91	2.95	2.96
Ag_6	1.50	1.50	-5.71	3.00	2.99	-0.01	6.95	6.94	1.27	1.30	2.84	2.82	7.02	7.02	1.21	1.24	2.91	2.89
Cu_7	1.63	1.82	-22.21	1.27	1.27	0	5.89	5.74	1.83	1.75	2.03	2.00	6.05	5.88	1.69	1.57	2.18	2.15
Cu_6Ag	1.57	1.77	-22.51	1.27	1.27	0	5.82	5.69	1.80	1.87	2.01	1.91	5.97	5.82	1.65	1.55	2.16	2.13
Cu_5Ag_2	1.51	1.73	-22.36	1.27	1.27	0	5.76	5.64	1.76	1.67	2.00	1.99	5.90	5.76	1.62	1.53	2.14	2.12
Cu_4Ag_3	1.45	1.69	-23.53	1.24	1.25	0.01	5.74	5.31	1.99	1.82	1.88	1.87	6.02	5.84	1.84	1.71	2.09	2.06
Cu_3Ag_4	1.38	1.63	-19.29	1.25	1.25	0	5.63	5.52	1.68	1.81	1.97	1.85	5.75	5.62	1.54	1.47	2.10	2.08
Cu_2Ag_5	1.32	1.56	-5.42	1.25	1.18	-0.07	5.56	4.96	1.64	1.94	1.96	1.51	5.68	5.23	1.51	1.21	2.08	2.01
$CuAg_6$	1.25	1.51	**-7.45**	1.21	1.23	0.02	5.67	5.13	1.80	2.04	1.94	1.54	5.79	5.38	1.65	1.27	2.07	2.06
Ag_7	1.17	1.44	-1.80	1.17	1.17	0	5.76	5.73	1.98	2.13	1.89	1.80	5.92	5.89	1.82	1.81	2.05	2.04
Cu_8	1.73	1.88	-20.46	3.30	3.03	-0.27	6.41	6.31	1.24	0.94	2.58	2.68	6.97	6.68	0.69	0.90	3.14	2.89
Cu_7Ag	1.69	1.85	-21.94	3.20	2.98	-0.22	6.38	6.50	1.03	0.98	2.55	2.76	6.96	6.65	1.15	0.93	2.99	2.86
Cu_6Ag_2	1.64	1.81	-19.74	3.16	2.90	-0.26	6.47	6.28	1.08	1.06	2.70	2.61	6.97	6.63	1.03	1.00	2.97	2.82
Cu_5Ag_3	1.60	1.78	**-18.14**	3.13	2.85	-0.28	6.78	6.46	1.13	1.12	2.83	2.67	6.92	6.62	1.08	1.06	2.92	2.78
Cu_4Ag_4	1.56	1.74	**-15.73**	3.10	2.80	-0.30	6.54	6.26	1.17	1.17	2.69	2.54	6.90	6.60	1.13	1.12	2.89	2.74
Cu_3Ag_5	1.48	1.68	**-12.73**	3.10	2.82	-0.28	6.44	6.21	1.17	1.16	2.63	2.53	6.90	6.59	1.11	1.10	2.90	2.75
Cu_2Ag_6	1.41	1.61	**-10.41**	3.09	2.83	-0.26	6.32	5.97	1.17	1.14	2.58	2.41	6.87	6.56	1.02	1.08	2.93	2.74
$CuAg_7$	1.33	1.55	**-7.12**	3.08	2.82	-0.26	6.19	6.37	1.13	1.25	2.40	2.56	6.87	6.55	1.06	1.06	2.90	2.75
Ag_8	1.26	1.49	-1.83	3.08	3.08	0	6.34	6.20	1.19	1.42	2.58	2.39	6.84	6.80	1.04	1.05	2.90	2.87

[a]Clusters, which show perpendicular H_2 adsorption, are highlighted in red, and those whose adsorption energies fall into the energy range between −6 and −18 kJ mol^{-1} are highlighted in green. Δ symbolizes the HLG difference between the bare and H_2-adsorbed clusters.

have the opposite trend as shown in $Cu_{(8-n)}Ag_n$, for example, in Figures 3 and 4, for a given size of a cluster. The average rates of the cluster expansion and binding energy lowering are about 0.043 Å and 0.059 eV per Ag atom substitution, respectively.

3.2. Hydrogen Adsorption on Clusters. We explored the hydrogen adsorption on Cu_mAg_n clusters extensively using the effect of the adsorption on the binding energy, average bond distances, hardness, HOMO−LUMO gap, properties of electronic energy states, and the vibrational frequencies of bare and adsorbed bimetallic clusters. The adsorption of a hydrogen molecule on each atom in a particular cluster was examined and then one that had the most favorable adsorption was reported. Tables 3 and 4 present all of the energy parameters and selected vibrational frequencies with corresponding bond lengths for both bare and hydrogen-adsorbed Cu_mAg_n clusters, respectively. Their structures and binding energy variation upon H_2 adsorption are shown in Figure S1 and Table S1 in the Supporting Information, respectively. The average binding energies of hydrogen-adsorbed copper-rich clusters are comparatively higher than those of silver-rich clusters of the same size (decrease in the binding energy with Ag substitution), indicating the higher stability of copper-rich systems over the silver-rich systems similar to the trend observed in bare Cu_mAg_n systems (Figure 4). The rate of the decrease in the average binding energy of a particular cluster

https://doi.org/10.1021/acsomega.1c06146
ACS Omega 2022, 7, 2316−2330

Table 4. Comparison of Calculated Average Nearest Neighbor Bond Distances ($\langle r \rangle$)/Å and the Minimum and Maximum Vibrational Frequencies (ν)/cm^{-1} of Both Bare and H_2-Adsorbed Clusters of Cu_mAg_n ($m + n = 2-8$) with Hydrogen−Hydrogen, Metal−Hydrogen Bond Distances, and Frequencies (ν)/cm^{-1} Corresponding to Those Hydrogen and Metal−Hydrogen Vibrational Modes[a]

Cluster	Average bond distance ($<r>$) /Å					Vibration frequency (ν)/cm^{-1}					
	Bare	Ads	H-H	M-H1	M-H2	H-H	M-H asym st	M-M_{min} bare	M-M_{min} H_2 ads	M-M_{max} bare	M-M_{max} H_2 ads
H_2	-	-	0.743	-	-	4417.7	-	-	-	-	-
Cu_2	2.259	2.279	0.770	1.765	1.766	3957.1	805.0	257.5	160.1	-	249.1
CuAg	2.433	2.438	0.771	1.765	1.765	3955.2	792.0	215.7	148.1	-	212.2
Ag_2	2.612	2.611	0.748	2.363	2.647	4315.4	243.5	177.6	57.3	-	178.0
Cu_3	2.326	2.409	0.792	1.687	1.680	3582.0	1169.2	53.4	64.0	237.9	238.6
Cu_2Ag	2.416	2.532	0.789	1.699	1.694	3639.3	1137.8	8.9	102.5	221.6	228.1
$CuAg_2$	2.504	2.657	0.787	1.705	1.705	3675.7	1087.0	14.0	83.2	200.9	198.0
Ag_3	2.69	2.811	0.759	2.136	2.137	4123.5	481.5	10.3	56.5	161.7	164.4
Cu_4	2.425	2.420	0.801	1.662	1.662	3461.3	1294.3	55.0	52.4	252.8	245.8
Cu_3Ag	2.492	2.488	0.799	1.666	1.672	3495.5	1273.2	50.3	48.1	247.3	240.1
Cu_2Ag_2	2.558	2.556	0.797	1.676	1.676	3529.8	1249.1	45.5	43.5	240.0	231.1
$CuAg_3$	2.672	2.668	0.798	1.678	1.678	3510.8	1244.1	41.7	39.2	208.0	199.1
Ag_4	2.784	2.780	0.768	2.037	2,038	3977.9	711.3	34.9	33.7	175.4	173.8
Cu_5	2.438	2.440	0.780	1.753	1.741	3763.5	994.2	37.9	26.6	243.9	245.7
Cu_4Ag	2.494	2.490	0.782	1.746	1.735	3744.3	1021.1	37.2	26.5	233.8	236.3
Cu_3Ag_2	2.534	2.539	0.780	1.758	1.739	3765.3	999.6	34.8	26.5	216.4	219.1
Cu_2Ag_3	2.612	2.618	0.780	1.754	1.743	3774.6	992.6	30.9	23.7	216.0	217.8
$CuAg_4$	2.693	2.692	0.744	2.687	3.423	**4375.7**	**347.1**	25.5	26.0	209.5	208.8
Ag_5	2.801	2.798	0.742	3.244	3.942	4401.3	374.9	25.4	25.9	170.3	170.9
Cu_6	2.440	2.440	0.745	2.791	3.452	**4347.0**	**317.9**	33.1	37.8	248.5	248.1
Cu_5Ag	2.477	2.480	0.760	1.890	1.900	**4127.2**	**516.1**	34.3	35.8	249.1	243.6
Cu_4Ag_2	2.514	2.516	0.760	1.884	1.905	**4124.7**	**460.8**	33.9	35.3	243.2	237.7
Cu_3Ag_3	2.552	2.550	0.744	2.862	3.525	**4360.6**	**342.0**	32.5	34.0	225.7	226.7
Cu_2Ag_4	2.634	2.632	0.743	2.932	3.608	**4376.6**	**309.5**	26.6	27.7	224.9	225.9
$CuAg_5$	2.743	2.730	0.774	1.787	1.787	3876.3	878.2	26.9	24.4	228.4	199.2
Ag_6	2.800	2.797	0.742	3.364	4.027	4404.5	304.5	25.9	27.1	176.5	176.9
Cu_7	2.517	2.519	0.767	1.812	1.812	3992.3	767.4	54.4	48.0	215.4	217.3
Cu_6Ag	2.564	2.563	0.768	1.808	1.809	3985.7	785.0	42.2	32.6	213.3	215.0
Cu_5Ag_2	2.609	2.608	0.768	1.819	1.818	3987.5	776.2	33.0	26.5	210.5	212.2
Cu_4Ag_3	2.661	2.613	0.774	1.777	1.777	3882.7	913.4	40.9	43.1	203.1	204.9
Cu_3Ag_4	2.698	2.699	0.768	1.815	1.816	3986.2	773.4	19.6	14.8	193.1	195.0
Cu_2Ag_5	2.770	2.760	0.766	1.857	1.854	4006.7	729.8	14.0	15.4	178.7	170.8
$CuAg_6$	2.817	2.827	0.763	1.891	1.890	**4048.8**	**657.5**	26.9	5.1	164.7	167.3
Ag_7	2.887	2.888	0.745	2.586	3.331	4339.6	372.9	38.6	34.1	149.4	149.4
Cu_8	2.509	2.512	0.766	1.843	1.853	4000.8	690.3	48.7	23.0	211.8	212.6
Cu_7Ag	2.538	2.540	0.768	1.836	1.827	3976.1	741.9	48.7	47.5	212.0	210.5
Cu_6Ag_2	2.567	2.569	0.767	1.835	1.839	3987.0	739.9	41.0	43.6	212.1	210.6
Cu_5Ag_3	2.592	2.599	0.767	1.828	1.847	**3984.3**	**749.8**	38.8	40.3	211.3	209.6
Cu_4Ag_4	2.625	2.628	0.767	1.842	1.844	**3995.2**	**747.9**	36.4	37.8	199.9	202.6
Cu_3Ag_5	2.687	2.691	0.764	1.866	1.874	**4031.5**	**695.5**	34.5	35.5	193.2	193.2
Cu_2Ag_6	2.750	2.754	0.765	1.874	1.881	**4023.3**	**700.9**	31.7	33.9	184.2	175.9
$CuAg_7$	2.812	2.816	0.762	1.921	1.913	**4070.9**	**630.8**	32.2	33.6	187.9	156.9
Ag_8	2.874	2.873	0.744	2.731	3.475	4358.2	273.7	32.2	26.8	147.0	146.1

[a]Clusters, which show perpendicular H_2 adsorption, are highlighted in red, and those whose adsorption energies fall into the energy range between −6 and −18 kJ mol^{-1} are highlighted in green.

size with silver composition is higher for the bare clusters than for hydrogen-adsorbed clusters, and also, this decrease in the rate decreases with the cluster size (Figure S3: 0.095 eV for $m + n = 2$ while 0.05 eV for $m + n = 8$ per substitution). On the

https://doi.org/10.1021/acsomega.1c06146
ACS Omega 2022, 7, 2316−2330

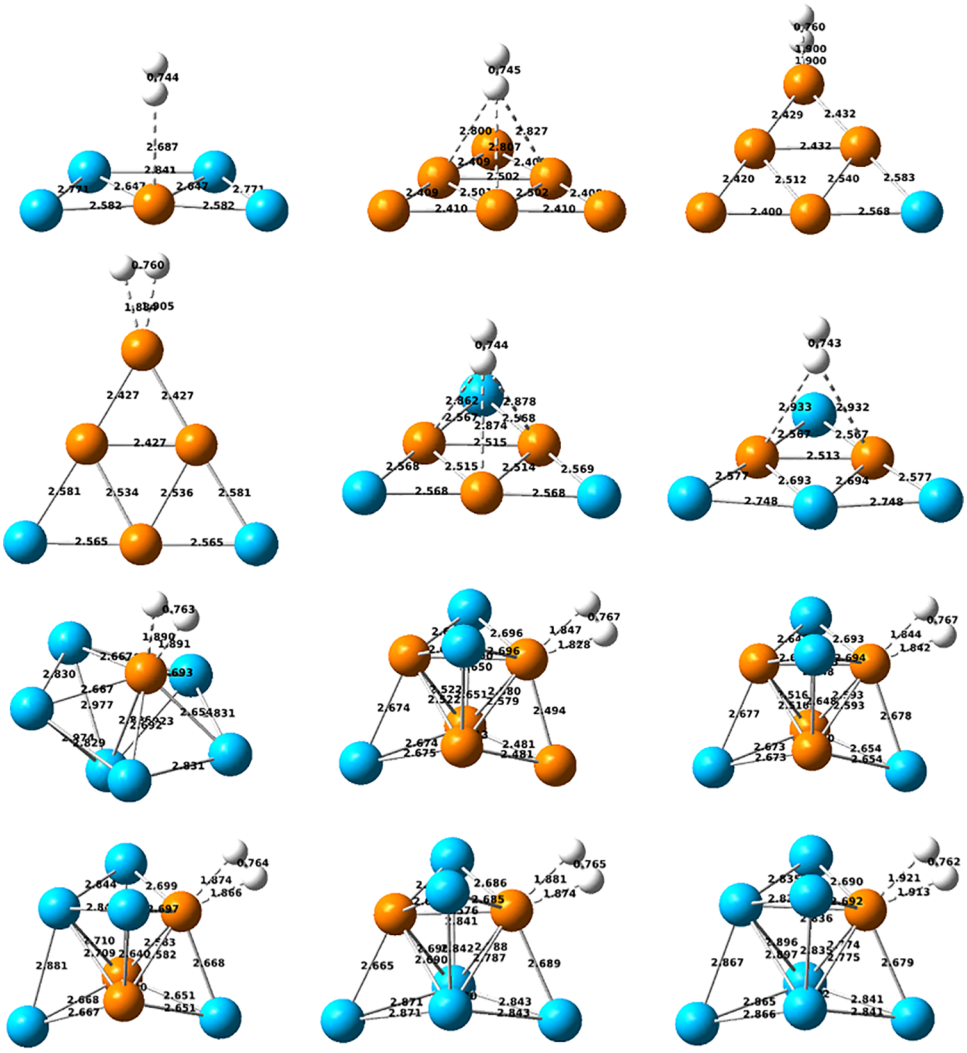

Figure 5. Structures of H_2-adsorbed clusters that are in the adsorption energy range of −6 to −18 kJ mol^{-1} in the order of $CuAg_4$, Cu_6, Cu_5Ag Cu_4Ag_2, Cu_3Ag_3, Cu_2Ag_4, $CuAg_6$, Cu_5Ag_3, Cu_4Ag_4, Cu_3Ag_5, Cu_2Ag_6, and $CuAg_7$ from top left to bottom right. Color notation: copper atoms in orange and silver atoms in blue.

other hand, the binding energy difference given in Table S1, which accounts for the extra binding energy per atom added to the cluster due to the adsorption of a hydrogen molecule (two hydrogen atoms), decreases with the increase of cluster sizes as it is an average over the entire cluster.

Here, we first summarize the best cluster candidates found in this study and then discuss the scientific base pieces of evidence to clarify the result. According to the U.S. Department of Energy Standard,[56] physisorption-based materials have been identified as good candidates for a hydrogen storage system. For optimum adsorption capacity of the storage system, the adsorption enthalpy between hydrogen molecules and materials should be less than −18 kJ mol^{-1} to meet the lower (3 atm) and upper (100 atm) pressures of the storage tank at the ambient temperature, respectively, and also, it should be higher than −6 kJ mol^{-1}. The adsorption enthalpies given in Table 3 and their variations with copper composition for each cluster reveal the tunable capacity of bimetallic clusters that meet the above optimum standard. A previous study by Fang et al. on hydrogen molecular adsorption on Pt-doped gold clusters also found similar behavior.[30] All Cu_n clusters (except Cu_6, discussed below) have larger adsorption enthalpies falling in the range of chemisorption, while Ag_n clusters have much smaller values, which are even below the lower limit of physisorption (except Ag_4) at which almost all hydrogen molecules stay unbound to the material. Smaller Cu_mAg_n clusters up to the hexamer, except $CuAg_4$, show much higher adsorption enthalpies than the recommended optimum value of −18 kJ mol^{-1} but, interestingly, some of the heterogeneous clusters of the hexamer and above, which are highlighted in green in Table 3, fall in the range of −6 to −18 kJ mol^{-1}, namely, the clusters $CuAg_4$, Cu_6, Cu_5Ag, Cu_4Ag_2, Cu_3Ag_3, Cu_2Ag_4, $CuAg_6$, Cu_5Ag_3, Cu_4Ag_4, Cu_3Ag_5, Cu_2Ag_6, and $CuAg_7$, shown in Figure 5.

The HOMO−LUMO gap (HLG) and chemical hardness values calculated (eq 7) using both adiabatic (η_a) and vertical (η_v) processes of the substance, which have a similar meaning, give information about the chemical reactivity of the clusters; it measures how a substance shows resistance to a change in its electron distribution.[57−59]

As shown in Table 3, HLG shows an odd−even fluctuation in the series from n = 2 to 8 that the clusters with an even number of atoms have higher values than the cluster with an odd number of atoms. As a general trend, HLG decreases with the silver substitution in the same cluster. These trends are common for both bare and hydrogen-adsorbed cluster series.

https://doi.org/10.1021/acsomega.1c06146
ACS Omega 2022, 7, 2316−2330

Some correlation between HLG and the H_2 adsorption energy can be observed. The clusters, which have larger adsorption energy over −55 kJ mol^{-1}, show considerably lower HLG values than the corresponding H_2-adsorbed clusters, namely, Cu_4, Cu_3Ag, Cu_2Ag_2, and $CuAg_3$. The HLG differences, Δ shown in Table 3, are as large as 0.8 eV for these clusters. The clusters with moderate hydrogen adsorption energy, generally between −19 and −55 kJ mol^{-1}, except most of the neat silver clusters (Ag_2, Ag_3, Ag_5, Ag_6, Ag_7, and Ag_8) and silver-rich clusters with silver more than 70% ($CuAg_6$, Cu_2Ag_5, and $CuAg_4$), have HLG values still lower than those of their hydrogen-adsorbed counterparts with the difference (Δ) less than 0.7 eV. The most interesting fact is that the clusters that are named good candidates for hydrogen storage materials have HLG values similar to or even greater than their hydrogen-adsorbed counterparts ($\Delta \leq 0.1$), indicating the intact electron distribution of the cluster material upon H_2 adsorption. Chemical hardness calculated using the vertical processes (η_v) is higher than that calculated using adiabatic processes (η_a), in which the relaxation of ionic clusters after removal and gain of an electron is considered. While observing a similar trend of HLG to the chemical hardness, as expected because of the qualitatively same parameters calculated in different ways, chemical hardness exhibits higher numerical values than the HLG except for the hexamer and the octamer, which show the opposite. The practical use of these parameters, HLG and chemical hardness, one over the other is more substance-specific, and more information can be found elsewhere.[35]

The adsorption strengths were further distinguished using the vibrational frequency and corresponding bond distance analysis. Table 4 summarizes the average bond distances of the clusters before and after the adsorption of the H_2 molecule, metal−hydrogen bond distances, minimum and maximum vibrational frequencies of both bare and hydrogen-adsorbed clusters, hydrogen−hydrogen frequency, and metal−hydrogen frequency. The orientation or the approach of the H_2 molecule upon adsorption to the cluster occurs in two different ways: either by perpendicular (only one of two hydrogen atoms interacts with the cluster) or by parallel (both hydrogen atoms interact with the cluster) to the cluster. Perpendicular orientation is defined using MH_1 and MH_2 bond lengths that the MH_2 bond length is the sum of the MH_1 bond length plus the approximate bond distance of a free H_2 molecule (≈0.7Å) while parallel adsorption is defined as the adsorption with equal or closer bond lengths of MH_1 and MH_2. A comparison of Tables 3 and 4 and the structures in Figure S1 reveal that the perpendicular orientation of the H_2 molecule (marked red in Tables 3 and 4) has reduced adsorption energy and is predominantly in silver-rich clusters except for Cu_6. Among them, the neat silver clusters are almost unbound to the H_2 molecules and the mixed systems, $CuAg_4$, Cu_3Ag_3, and Cu_2Ag_4, have no vertex Cu atom. Perpendicular orientation in the Cu_6 cluster, which has three vertices of Cu atoms, may be due to the geometry of the cluster. The geometry of the original cluster is D_{3h} and perpendicular adsorption reduces it only to C_{3v}, while parallel adsorption would reduce it further. This results in lower adsorption energy compared to the other copper neat clusters. Three predominant features from hydrogen adsorption data and structures can be drawn: (1) favorable adsorption on the cluster vertex Cu atom, (2) unfavorable interaction to Ag atoms, and (3) high symmetry adaptation. Up to the pentamer, heterogeneous clusters have at least one vertex Cu atom in the cluster except for $CuAg_4$ and also can adopt some symmetry on parallel adsorption. Therefore, we can observe high adsorption energy. In the case of $CuAg_4$, it favors the perpendicular adsorption to maintain a sort of symmetry. Adsorption on all clusters of the heptamer and octamer, except on Ag_7 and Ag_8 on which no adsorption was observed, is parallel. They all have at least one vertex Cu atom and reduced symmetry, which would not be affected effectively on adsorption. These observations can be summarized as the adsorption of the H_2 molecule noticeably favors the sites, where the most positively charged environment persists. H_2 molecule adsorbs onto either the most positively charged copper atoms (or reaches onto the most positive silver atom in Ag_n monometallic clusters) at the vertices of the cluster or the site which has the most positive charge environment avoiding the negatively charged atoms in the vicinity as also observed in previous studies, especially that the H_2 adsorption occurred on top of the most positively charged three-coordinated Cu atom in the small diagonal of Cu_4 rhombus.[31,32] With the adsorption, the positive charge density of the adsorbed atom or the atom closer to the adsorbed site decreases, acquiring more negative charge density. We will discuss the electron distributions further in the natural bond orbital (NBO) analysis below.

As we mentioned above, there is no change in the bond distance of the H_2 molecule in the perpendicular adsorption, while the elongation of the H_2 bond distance can be observed in the parallel adsorption. Stronger metal−H_2 interactions cause the MH_1 and MH_2 distances shorter with the H_2 bond elongation. Among the cluster species selected as candidates for the hydrogen storage system, the interactions between H_2 and $CuAg_4$, Cu_6, Cu_3Ag_3, and Cu_2Ag_4 species do not affect the H−H bond distance, and the metal−hydrogen distance is comparatively longer, while the rest, Cu_5Ag, Cu_4Ag_2, $CuAg_6$, Cu_5Ag_3, Cu_4Ag_4, Cu_3Ag_5, Cu_2Ag_6, and $CuAg_7$, make interactions with both hydrogen atoms of the molecule causing a longer H−H distance and metal−hydrogen distance is about 1 Å shorter than the former. The frequencies of H−H and the M−H modes show the same observations as expected relevant to the bond distance change (marked green in Table 4) upon adsorption. The effect of hydrogen adsorption on metal−metal interactions can also be understood by comparing the minimum and maximum frequencies of the metal−metal vibrational modes before and after the adsorption since all of the other modes are within these two extremes. At the lower end of the cluster series (especially, $m + n = 2$ and 3 clusters), there are observable changes in vibrational modes, but when the cluster size increases, in general, the differences are not in a smooth pattern and become smaller. The minimum frequency modes show a red shift (lower frequency) in $m + n = 2$ clusters, while $m + n = 3$ clusters show a blue shift (lager frequency) upon H_2 adsorption, reflecting the differences in adsorption energies of two species. In the clusters of $m + n = 4$, both minimum and maximum frequency modes are red-shifted as the observation made for the $Cu_nPt_{(4-n)}$ ($n = 0-4$) clusters by Gálvez-González et al.[32] In contrast to the literature on dissociative hydrogen adsorption on some of Au_nPt clusters reported by Gálvez-González et al.[32] and Fang and Kuang,[30] some cationic Pt clusters reported by Kerpal et al.,[60] and some Au_n clusters reported by Fang and Kuang[30] and Molina et al.,[61] nondissociative adsorptions of H_2 on the entire series of Cu_mAg_n for ($m + n \leq 8$) clusters were observed.

https://doi.org/10.1021/acsomega.1c06146
ACS Omega 2022, 7, 2316−2330

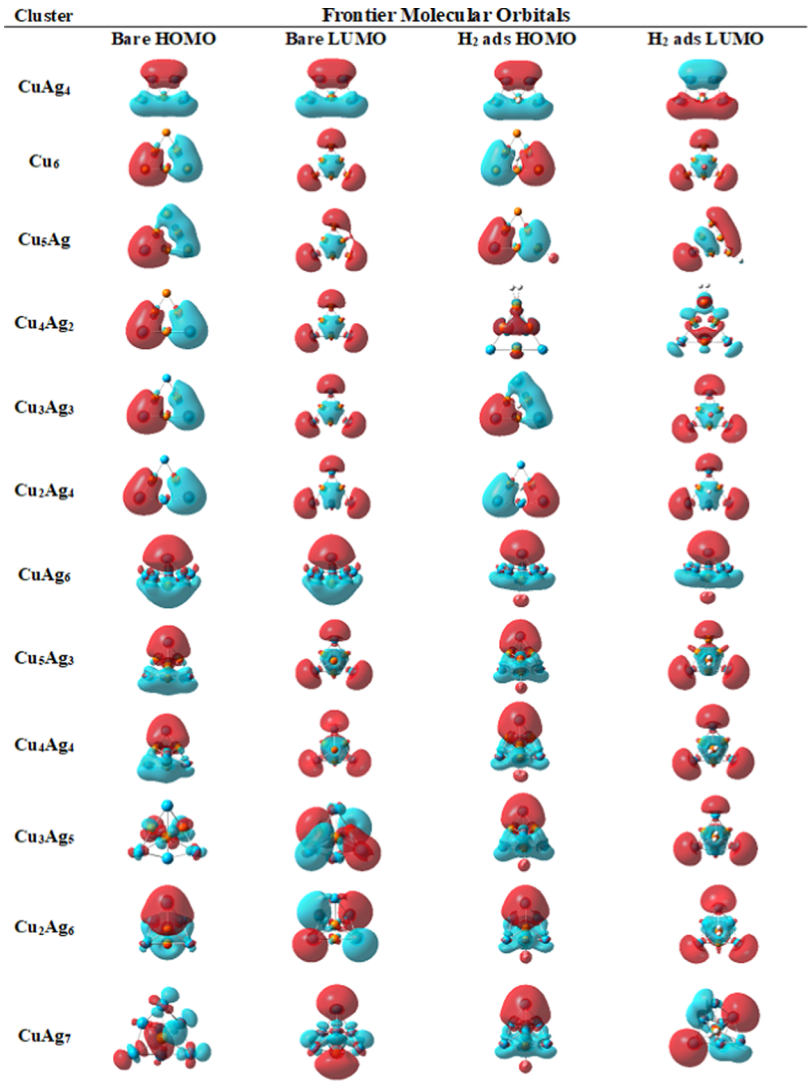

Figure 6. Spatial distributions of HOMO and LUMO frontier molecular orbitals of 12 clusters identified as candidates for hydrogen storage materials: red and blue color lobes correspond to the two different phases of the orbital wave function with positive and negative signs, respectively.

3.3. Electronic Structure Change and Charge Transfer Processes. The natural bond orbital (NBO) analysis for those 12 clusters was performed to understand their electron redistributions and charge transfer process at the formation of the cluster and also on H_2 adsorption. Both intra- and interatomic charge transfer within the cluster and adsorbed H_2 molecules could be observed. For each cluster, spatial distributions of HOMO and LUMO frontier orbitals and the natural electron configuration of constituent elements, which give the occupancies of atomic orbitals,[62] with their natural charge distribution are given in Figure 6 and Table S2 in the Supporting Information, respectively. The electron configuration of free atoms, Cu, Ag, and H, is $[Ar]3d^{10}4s^1$, $[Kr]4d^{10}5s^1$, and $1s^1$, respectively. Inner core notations, [Ar] and [Kr], will be dropped hereon for easy presentation.

Cu_6: It has a planar triangle structure consisting of copper atoms with two different electron configurations, $3d^{9.93}4s^{0.90}4p^{0.02}$ for the three atoms at the vertices and $3d^{9.92}4s^{0.82}4p^{0.40}$ for the three atoms along the sides of the triangle. All six Cu atoms in the cluster molecule show spd hybridization with intra-atomic charge transfer from 4s and 3d to 4p in contrast to the charge transfer process reported in this study and literature for Cu_4.[31] In Cu_4, the two Cu atoms on the short diagonal promoted electrons from 4s and 3d to 4p, while those of the long diagonal promoted electrons from 3d to 4s. In addition, these electron configurations give further insight into interatomic charge transfer between the atoms in the cluster. Each atom at the vertices lost 0.143 electrons, leaving it positively charged, while each atom along the sides gained 0.143 electrons and hence became negatively charged. The spd hybridization and then the intra- and interatomic charge transfer give stability to the cluster.[63] Moving onto the H_2-adsorbed Cu_6, there is no accountable intermolecule charge transfer between the H_2 molecule and Cu_6 cluster but an induced dipole moment on the H_2 molecule by the Cu_6–dipole can be observed. With the hydrogen adsorption, while there is no further intra-atomic charge transfer taking place, interatomic charge transfer from the 4s orbital of the Cu atoms at the vertices to 4p orbitals of the Cu atoms on the sides of the triangle takes place; each Cu atom at the vertices loses 0.03 electrons with the result of 0.03 electrons gained by each Cu atom on three sides. This process has further enhanced the already existing charge separation on the cluster. In parallel to this process, the H_2 molecule also becomes polarized in

https://doi.org/10.1021/acsomega.1c06146
ACS Omega 2022, 7, 2316−2330

accumulating electrons to the H atom closer to the cluster surface ($1s^{1.01}2s^{0.01}$) and leaving the other atom electron-deficient ($1s^{0.98}$). As we discussed above by bond distance and vibrational frequency analysis, the H_2 reaching out to Cu_6 as perpendicular adsorption (Figure 5) is further confirmed by this charge transfer analysis. Therefore, the hydrogen adsorption arises only due to the induced dipole interaction, which results in physisorption (−16.71 kJ mol^{-1}, Table 3) but not due to the charge transfer between the H_2 molecule and the cluster.

Cu_5Ag: All atoms in the cluster show spd hybridizations similar to Cu_6 with intra-atomic charge transfer from 4s and 3d to 4p in the five Cu atoms and from 5s and 4d to 5p in the Ag atom. Interatomic charge transfer is unsymmetrical compared to that of Cu_6 as a result of Ag substitution (Table S2 in the Supporting Information). The Ag atom has been substituted to one of three vertices as discussed in Section 3.2 due to its larger size and enhanced electron negativity. All three atoms at the vertices (2 Cu, Ag) donated electrons to the three atoms on the sides. The transfer of electrons from Ag ($4d^{9.96}5s^{0.91}5p^{0.02}$) is less compared to the transfer from the two Cu atoms ($3d^{9.93}4s^{0.89}4p^{0.02}$); this is in accordance with the higher electron negativity of Ag compared to Cu. The two Cu atoms ($3d^{0.92}4s^{0.82}4p^{0.39}$) on two sides bonded to the Ag atom gained fewer electrons for the same reason. Therefore, accumulations of the electrons are more predominant on the Cu atom on the side connecting two vertex Cu atoms ($3d^{0.92}4s^{0.83}4p^{0.41}$).

In the case of H_2 adsorption, the H_2 molecule lost 0.04 electrons (0.02 from each hydrogen: $1s^{0.98}$), which were gained by the cluster. The total charge of the cluster becomes negative (−0.027) equally to the positive charge of the H_2 molecule (+0.028); this slight difference arises from the error due to the round-off of the charge values to the third decimal point (Table S2 in the Supporting Information). Then, the cluster−H_2 molecule interaction can be considered as a weak ionic interaction with −15.89 kJ mol^{-1} physisorption energy. This charge transfer upon H_2 adsorption caused the redistribution of electrons in the cluster while the electron-deficient H_2 molecule remains unpolarized. Three atoms at the vertices now become less positive as a result of the rearranging of both the 0.04 electrons pumped to the cluster and electrons within the cluster. The positive charge of the vertex Cu atom (labeled Cu-4), where the H_2 molecule was adsorbed, changed from 0.148 to 0.101 with 0.06 electrons gained from interatomic electron transfer and also with the electron promotion from 4s and 3d to 4p, and its electronic state was rearranged from $3d^{9.93}4s^{0.89}4p^{0.02}$ to $3d^{9.90}4s^{0.85}4p^{0.15}$. The other vertex Cu atom gained 0.04 electrons only by the interatomic charge transfer during the adsorption with the enhanced enrollment of 4s orbital and 5s orbital, [($3d^{9.93}4s^{0.89}4p^{0.02}$) → ($3d^{9.93}4s^{0.92}4p^{0.02}5s^{0.01}$)], which changed the atomic charge from 0.148 to 0.123. Similarly, in the third vertex atom, Ag, only the 5s orbital gained 0.03 electrons to reduce the charge from 0.148 to 0.091. In addition, one of three Cu atoms on sides also gained 0.01 electrons to its 4s atomic orbital while only two vertex Cu atoms donated 0.09 electrons to the entire system. This charge transfer analysis and hence the weak ionic interaction between the cluster and the H_2 molecule justify the identified parallel adsorption of the H_2 molecule in the previous section based on the bond distance and vibrational analysis.

HOMO−LUMO frontier orbital diagrams (Figure 6) also depict the induced dipole interaction of the H_2 molecule with the Cu_6 cluster as perpendicular adsorption and weak ionic interaction of the H_2 molecule to the Cu_5Ag cluster as parallel adsorption. In Cu_6, the FMO shapes of the HOMO and LUMO of H_2-adsorbed clusters are similar to those of the HOMO and LUMO before the adsorption. Two phases (opposite phases of the orbital donated by red and blue) of the HOMO concentrated around the two vertex Cu atoms (blue and red color in the diagram), leaving the Cu atom on the side connecting these two vertexes and the Cu atom remaining at the third vertex. These two opposite phases have created a narrow hollow region inside the triangle. In contrast, the LUMO, which is responsible for attracting electrons from the HOMO of another molecule, has no hollow region; instead, one of the two phases (blue) resides at the center of the cluster (inside the triangle) and the other phase (red) is concentrated separately at three vertices as three separate lobes. This shape of the LUMO influences the H_2 molecule reaching perpendicularly toward the center of the triangle and induced the electron density of the H_2 molecules to be polarized. The same shapes of HOMO and LUMO frontier molecular orbitals after the adsorption of H_2 molecules revealed that there is no charge transfer between the H_2 molecule and the cluster, and hence, the induced dipole interaction takes place as discussed before.

But in the case of Cu_5Ag, where we identified H_2 adsorption to the cluster due to a weak ionic interaction and as parallel adsorption, the FMO shapes of the HOMO and LUMO before and after the H_2 adsorption are different. In the bare cluster, two vertex atoms, Cu and Ag, and the Cu atom on the side connecting these two atoms are clouded by one lobe of two opposite phases of the FMO (blue) and the remaining lobe (red) resides at the remaining vertex, leaving the vicinity of two Cu atoms on the other two sides and the center of the triangle free of electron density. The LUMO appears to be the same as the LUMO of Cu_6, indicating good electron acceptance capacity. In Cu_5AgH_2 (after the H_2 adsorption), the HOMO and LUMO are completely different from those of the bare cluster, confirming the electron transfer from the H_2 molecule to the cluster and also the redistributions of electrons. In the HOMO, electrons are localized on the atoms away from the Ag atom, and in the LUMO, they are lobbied on the vertex atoms including Ag.

Continuation of the discussion on atomic orbital occupancy and FMO analysis for the remaining 10 clusters, $CuAg_4$, Cu_4Ag_2, Cu_3Ag_3, Cu_2Ag_4, $CuAg_6$, Cu_5Ag_3, Cu_4Ag_4, Cu_3Ag_5, Cu_2Ag_6, and $CuAg_7$, will find the same pattern of behavior, confirming the hydrogen adsorption characteristic identified in Section 3.2. The clusters identified with perpendicular adsorptions, $CuAg_4H_2$, Cu_6H_2, $Cu_3Ag_3H_2$, and $Cu_2Ag_4H_2$, have no charge transfer between the H_2 molecule and the cluster and polarize the H_2 molecule; hence, their H_2 adsorptions are due to the induced dipole interactions. On the other hand, the remaining six clusters, Cu_5AgH_2, $Cu_4Ag_2H_2$, $CuAg_6H_2$, $Cu_5Ag_3H_2$, $Cu_4Ag_4H_2$, $Cu_3Ag_5H_2$, $Cu_2Ag_6H_2$, and $CuAg_7H_2$, identified with parallel adsorption, have charge transfer between the H_2 molecule and the cluster and pull the electrons from the H_2 molecule; hence, their H_2 adsorptions are due to the ionic interactions.

https://doi.org/10.1021/acsomega.1c06146
ACS Omega 2022, 7, 2316−2330

4. CONCLUSIONS

In the search for potential candidates for hydrogen storage, Cu_mAg_n clusters for $m + n \leq 8$ were explored. The dimension transitions of both copper and silver cluster structures occur when the cluster size increases. The dimer is a 1-D structure, whereas the trimer to the hexamer possess planar 2-D structure patterns and the clusters above the hexamer are in 3-D arrangements. The clusters of both pure Cu_n and Ag_n have the shapes of an isosceles triangle for the trimer, rhombus for the tetramer, trapezoid for the pentamer, triangle for the hexamer, pentagonal bipyramid for the heptamer, and tetracapped tetrahedron for the octamer. With the heterogeneity, the Cu atoms tend to have maximum coordination within the cluster and the stability of copper clusters is relatively higher than that of the silver clusters. Hydrogen adsorptions to the clusters are observed with two general mechanisms, hydrogen is either parallel or perpendicular to the clusters. In the perpendicular reach, clusters polarized the H_2 molecule and there is no charge transfer process between the cluster and H_2 molecule and hence the adsorption is due to an induced dipole interaction. On the other hand, in parallel reach, the charge transfer between the H_2 molecule and cluster takes place and hydrogen donates electrons to the cluster. The cluster becomes negatively charged and the H_2 molecule becomes positively charged, resulting in weak ionic interactions between two entities. The adsorption is due to this ionic interaction. The H_2 adsorption energies of the entire series reveal that out of all of the candidates, only $CuAg_4$, Cu_6, Cu_5Ag, Cu_4Ag_2, Cu_3Ag_3, Cu_2Ag_4, $CuAg_6$, Cu_5Ag_3, Cu_4Ag_4, Cu_3Ag_5, Cu_2Ag_6, and $CuAg_7$ fall within the recommended energy range of −6 to −18 kJ mol^{-1} for hydrogen storage materials. The H_2 adsorption on the first four of 12 entities is due to the induced dipole interactions, while that on the remaining eight entities is due to the ionic interactions.

■ ASSOCIATED CONTENT

Supporting Information

The Supporting Information is available free of charge at https://pubs.acs.org/doi/10.1021/acsomega.1c06146.

Structures of hydrogen-adsorbed Cu_mAg_n clusters; average binding energy of bare and H_2-adsorbed Cu_mAg_n clusters; lowest energy and low-lying isomers of Cu_mAg_n clusters; variation of binding energy of H_2-adsorbed Cu_mAg_n clusters with silver substitution; and valence−shell electron configurations and the natural atomic charge on constituent elements of bare and hydrogen-adsorbed Cu_mAg_n clusters (PDF)

■ AUTHOR INFORMATION

Corresponding Author

Jinasena W. Hewage − *Department of Chemistry, University of Ruhuna, Matara 81000, Sri Lanka;* orcid.org/0000-0001-7713-7484; Phone: +94 71 450 0389; Email: jinasena@chem.ruh.ac.lk

Authors

Sathya M. Perera − *Department of Chemistry, University of Ruhuna, Matara 81000, Sri Lanka; School of Chemical and Biomolecular Sciences, Southern Illinois University, Carbondale, Illinois 62901, United States*

Samanthika R. Hettiarachchi − *Department of Chemistry, The Open University of Sri Lanka, Nawala 10250, Sri Lanka*

Complete contact information is available at: https://pubs.acs.org/10.1021/acsomega.1c06146

Notes

The authors declare no competing financial interest.

■ ACKNOWLEDGMENTS

We thank the Faculty of Science, University of Ruhuna, for continuous support of our work, and the National Research Council, Sri Lanka, for the initial financial support.

■ REFERENCES

(1) Rosi, N. L.; Eckert, J.; Eddaoudi, M.; Vodak, D. T.; Kim, J.; O'Keeffe, M.; Yaghi, O. M. Hydrogen Storage in Microporous Metal-Organic Frameworks. *Science* **2003**, *300*, 1127−1129.

(2) Rowsell, J. L. C.; Millward, A. R.; Park, K. S.; Yaghi, O. M. Hydrogen Sorption in Functionalized Metal−Organic Frameworks. *J. Am. Chem. Soc.* **2004**, *126*, 5666−5667.

(3) Panella, B.; Hönes, K.; Müller, U.; Trukhan, N.; Schubert, M.; Pütter, H.; Hirscher, M. Desorption Studies of Hydrogen in Metal−Organic Frameworks. *Angew. Chem., Int. Ed.* **2008**, *47*, 2138−2142.

(4) Schmitz, B.; Müller, U.; Trukhan, N.; Schubert, M.; Férey, G.; Hirscher, M. Heat of Adsorption for Hydrogen in Microporous High-Surface-Area Materials. *ChemPhysChem.* **2008**, *9*, 2181−2184.

(5) Dincă, M.; Long, J. R. Hydrogen Storage in Microporous Metal-Organic Frameworks with Exposed Metal Sites. *Angew. Chem., Int. Ed.* **2008**, *47*, 6766−6779.

(6) Dybtsev, D.; Serre, C.; Schmitz, B.; Panella, B.; Hirscher, M.; Latroche, M.; Llewellyn, P. L.; Cordier, S.; Molard, Y.; Haouas, M.; et al. Influence of $[Mo_6Br_8F_6]^{2-}$ Cluster Unit Inclusion within the Mesoporous Solid MIL-101 on Hydrogen Storage Performance. *Langmuir* **2010**, *26*, 11283−11290.

(7) Szilágyi, P. Á.; Weinrauch, I.; Oh, H.; Hirscher, M.; Juan-Alcañiz, J.; Serra-Crespo, P.; De Respinis, M.; Treześniewsk, B. J.; Kapteijn, F.; Geerlings, H.; et al. Interplay of Linker Functionalization and Hydrogen Adsorption in the Metal−Organic Framework Mil-101. *J. Phys. Chem. C* **2014**, *118*, 19572−19579.

(8) Szilágyi, P. Á.; Rogers, D. M.; Zaiser, I.; Callini, E.; Turner, S.; Borgschulte, A.; Züttel, A.; Geerlings, H.; Hirscher, M.; Dam, B. Functionalised Metal−Organic Frameworks: A Novel Approach to Stabilising Single Metal Atoms. *J. Mater. Chem. A* **2017**, *5*, 15559−15566.

(9) Allendorf, M. D.; Hulvey, Z.; Gennett, T.; Ahmed, A.; Autter, T.; Camp, J.; Seon Cho, E.; Furukawa, H.; Haranczyk, M.; Head-Gordon, M.; et al. An Assessment of Strategies for the Development of Solid-State Adsorbents for Vehicular Hydrogen Storage. *Energy Environ. Sci.* **2018**, *11*, 2784−2812.

(10) Makepeace, J. W.; He, T.; Weidenthaler, C.; Jensen, T. R.; Chang, F.; Vegge, T.; Ngene, P.; Kojima, Y.; De Jongh, P. E.; Chen, P.; et al. Reversible Ammonia-Based and Liquid Organic Hydrogen Carriers for High-Density Hydrogen Storage: Recent Progress. *Int. J. Hydrogen Energy* **2019**, *44*, 7746−7767.

(11) Christensen, C. H.; Johannessen, T.; Sørensen, R. Z.; Nørskov, J. K. Towards an Ammonia-Mediated Hydrogen Economy? *Catal. Today* **2006**, *111*, 140−144.

(12) Aakko-Saksa, P. T.; Cook, C.; Kiviaho, J.; Repo, T. Liquid Organic Hydrogen Carriers for Transportation and Storing of Renewable Energy − Review and Discussion. *J. Power Sources* **2018**, *396*, 803−823.

(13) Preuster, P.; Papp, C.; Wasserscheid, P. Liquid Organic Hydrogen Carriers (Lohcs): Toward a Hydrogen- Free Hydrogen Economy. *Acc. Chem. Res.* **2017**, *50*, 74−85.

(14) Yvon, K.; Renaudin, G. Hydrides: Solid State Transition Metal Complexes. In *Encyclopedia of Inorganic Chemistry*; King, R. B., Ed.; John Wiley & Sons, Ltd.: Chichester, 2006; pp 1814−1846.
(15) Humphries, T. D.; Sheppard, D. A.; Buckley, C. E. Recent Advances in the 18-Electron Complex Transition Metal Hydrides of Ni, Fe, Co and Ru. *Coord. Chem. Rev.* **2017**, *342*, 19−33.
(16) Callini, E.; Ageuy-Zinsou, K.-F.; Ahuja, R.; Ares, J. R.; Bals, S.; Billiškor, N.; Chakraborty, S.; Charalambopoulou, G.; Chaudhary, A.-L.; Cuevas, F.; et al. Nanostructured Materials for Solid-State Hydrogen Storage: A Review of the Achievement of Cost Action Mp1103. *Int. J. Hydrogen Energy* **2016**, *41*, 14404−14428.
(17) Callini, E.; Atakli, Z. O. K.; Hauback, B. C.; Orimo, S.-I.; Jensen, C.; Dornheim, M.; Grant, D.; Cho, Y. W.; Chen, P.; Hjörvarsson, B.; et al. Complex and Liquid Hydrides for Energy Storage. *Appl. Phys. A: Mater. Sci. Process.* **2016**, *122*, No. 353.
(18) Jepsen, L. H.; Ley, M. B.; Lee, Y.-S.; Cho, Y. W.; Dornheim, M.; Jensen, J. O.; Filinchuk, Y.; Jørgensen, J. E.; Besenbacher, F.; Jensen, T. R. Boron−Nitrogen Based Hydrides and Reactive Composites for Hydrogen Storage. *Mater. Today* **2014**, *17*, 129−135.
(19) Ley, M. B.; Jepsen, L. H.; Lee, Y.-S.; Cho, Y. W.; Bellosta Von Coble, J. M.; Dornheim, M.; Rokni, M.; Jensen, J. O.; Sloth, M.; Filinchuk, Y.; et al. Complex Hydrides for Hydrogen Storage − New Perspectives. *Mater. Today* **2014**, *17*, 122−128.
(20) Paskevicius, M.; Jepsen, L. H.; Schouwink, P.; Černý, R.; Ravnsbæk, D. B.; Filinchuk, Y.; Dornheim, M.; Besenbacher, F.; Jensen, T. R. Metal Borohydrides and Derivatives − Synthesis, Structure and Properties. *Chem. Soc. Rev.* **2017**, *46*, 1565−1634.
(21) Humphries, T. D.; Matsuo, M.; Li, G.; Orimo, S.-I. Complex Transition Metal Hydrides Incorporating Ionic Hydrogen: Thermal Decomposition Pathway of $Na_2Mg_2FeH_8$ and $Na_2Mg_2RuH_8$. *Phys. Chem. Chem. Phys.* **2015**, *17*, 8276−8282.
(22) Humphries, T. D.; Sheppard, D. A.; Li, G.; Rowles, M. R.; Paskevicius, M.; Matsuo, M.; Aguey-Zinsou, K.-F.; Sofianos, M. V.; Orimo, S.-I.; Buckley, C. E. Complex Hydrides as Thermal Energy Storage Materials: Characterisation and Thermal Decomposition of $Na_2Mg_2NiH_6$. *J. Mater. Chem. A* **2018**, *6*, 9099−9108.
(23) Takagi, S.; Orimo, S.-I. Recent Progress in Hydrogen-Rich Materials from the Perspective of Bonding Flexibility of Hydrogen. *Scr. Mater.* **2015**, *109*, 1−5.
(24) Tylianakis, E.; Dimitrakakis, G. K.; Melchor, S.; Dobado, J. A.; Froudakis, G. E. Porous Nanotube Network: A Novel 3-D Nanostructured Material with Enhanced Hydrogen Storage Capacity. *Chem. Commun.* **2011**, *47*, 2303−2305.
(25) Gotzias, A.; Tylianakis, E.; Froudakis, G.; Steriotis, T. Theoretical Study of Hydrogen Adsorption in Oxygen Functionalized Carbon Slit Pores. *Microporous Mesoporous Mater.* **2012**, *154*, 38−44.
(26) Stergiannakos, T.; Tylianakis, E.; Klontzas, E.; Trikalitis, P. N.; Froudakis, G. E. Hydrogen Storage in Novel Li-Doped Corrole Metal-Organic Frameworks. *J. Phys. Chem. C* **2012**, *116*, 8359−8363.
(27) Humphries, T. D.; Sheppard, D. A.; Buckley, C. E. Complex Transition Metal Hydrides: Linear Correlation of Countercation Electronegativity Versus T−D Bond Lengths. *Chem. Commun.* **2015**, *51*, 11248−11251.
(28) Hirscher, M.; Yartys, V. A.; Baricco, M.; Bellosta Von Colbe, J.; Blanchard, D.; Bowman, R. C.; Broom, D. P.; Buckley, C. E.; Chang, F.; Chen, P.; et al. Materials for Hydrogen-Based Energy Storage − Past, Recent Progress and Future Outlook. *J. Alloys Compd.* **2020**, *827*, No. 153548.
(29) Guvelioglu, G. H.; Ma, P.; He, X.; Forrey, R. C.; Cheng, H. Evolution of Small Copper Clusters and Dissociative Chemisorption of Hydrogen. *Phys. Rev. Lett.* **2005**, *94*, No. 026103.
(30) Fang, Z.; Kuang, X. Hydrogen Molecule Adsorption on Au_nPt (n = 1-12) Clusters in Comparison with Corresponding Pure Au_{n+1} (n = 1-12) Clusters. *Phys. Status Solidi B* **2014**, *251*, 446−454.
(31) Zhao, S.; Tian, X.; Liu, J.; Ren, Y.; Ren, Y.; Wang, J. Density Functional Study of Molecular Hydrogen Adsorption on Small Gold−Copper Binary Clusters. *J. Cluster Sci.* **2015**, *26*, 491−503.
(32) Gálvez-González, L. E.; Alonso, J. A.; Paz-Borbón, L. O.; Posada-Amarillas, A. H_2 Adsorption on $Cu_{4-x}M_x$ (M = Au, Pt; x = 0−4) Clusters: Similarities and Differences as Predicted by Density Functional Theory. *J. Phys. Chem. C* **2019**, *123*, 30768−30780.
(33) Frisch, M. J.; Trucks, G. W.; Schlegel, H. B.; Scuseria, G. E.; Robb, M. A.; Cheeseman, J. R.; Scalmani, G.; Barone, V.; Petersson, G. A.; Nakatsuji, H.et al.*Gaussian 16*, revision C.01; Gaussian, Inc.: Wallingford, CT, 2016.
(34) Hay, P. J.; Wadt, W. R. Ab Initio Effective Core Potentials for Molecular Calculations. Potentials for K to Au Including the Outermost Core Orbitals. *J. Chem. Phys.* **1985**, *82*, 299−310.
(35) Pearson, R. G. Chemical Hardness and Density Functional Theory. *J. Chem. Sci.* **2005**, *117*, 369−377.
(36) Pearson, R. G. The Principle of Maximum Hardness. *Acc. Chem. Res.* **1993**, *26*, 250−255.
(37) Pearson, R. G. Recent Advances in the Concept of Hard and Soft Acids and Bases. *J. Chem. Educ.* **1987**, *64*, 561−567.
(38) Parr, R. G.; Pearson, R. G. Absolute Hardness: Companion Parameter to Absolute Electronegativity. *J. Am. Chem. Soc.* **1983**, *105*, 7512−7516.
(39) Kuang, X.-J.; Wang, X.-Q.; Liu, G.-B. A Density Functional Study on the Adsorption of Hydrogen Molecule onto Small Copper Clusters. *J. Chem. Sci.* **2011**, *123*, 743−754.
(40) Lammers, U.; Borstel, G. Electronic and Atomic Structure of Copper Clusters. *Phys. Rev. B* **1994**, *49*, 17360−17377.
(41) Jackson, K. A. First-Principles Study of the Structural and Electronic Properties of Cu Clusters. *Phys. Rev. B* **1993**, *47*, 9715−9722.
(42) Massobrio, C.; Pasquarello, A.; Car, R. Structural and Electronic Properties of Small Copper Clusters: A First Principles Study. *Chem. Phys. Lett.* **1995**, *238*, 215−221.
(43) Kabir, M.; Mookerjee, A.; Bhattacharya, A. K. Structure and Stability of Copper Clusters: A Tight-Binding Molecular Dynamics Study. *Phys. Rev. A* **2004**, *69*, No. 043203.
(44) Leopold, D. G.; Ho, J.; Lineberger, W. C. Photoelectron Spectroscopy of Mass-Selected Metal Cluster Anions. I. Cu_n^-, n=1−10. *J. Chem. Phys.* **1987**, *86*, 1715−1726.
(45) Liao, M.-S.; Watts, J. D.; Huang, M.-J. Theoretical Comparative Study of Oxygen Adsorption on Neutral and Anionic Ag_n and Au_n Clusters (n = 2−25). *J. Phys. Chem. C* **2014**, *118*, 21911−21927.
(46) Beutel, V.; Krämer, H. G.; Bhale, G. L.; Kuhn, M.; Weyers, K.; Demtröder, W. High-Resolution Isotope Selective Laser Spectroscopy of Ag_2 Molecules. *J. Chem. Phys.* **1993**, *98*, 2699−2708.
(47) Srinivas, S.; Salian, U. A.; Jellinek, J. Theoretical Investigations of Silver Clusters and Silver-Ligand Systems. In *Metal−Ligand Interactions in Chemistry, Physics, and Biology*; Russo, N.; Salahub, D. R., Eds.; Springer: Dordrecht, 2000; pp 295−324.
(48) Morse, M. D. Clusters of Transition-Metal Atoms. *Chem. Rev.* **1986**, *86*, 1049−1109.
(49) Simard, B.; Hackett, P. A.; James, A. M.; Langridge-Smith, P. R. R. The Bond Length of Silver Dimer. *Chem. Phys. Lett.* **1991**, *186*, 415−422.
(50) Hilpert, K.; Gingerich, K. A. Atomization Enthalpies of the Molecules Cu_3, Ag_3, and Au_3. *Ber. Bunsen-Ges. Phys. Chem.* **1980**, *84*, 739−745.
(51) Wei-Yin, L.; Sha, Z.; Lian, H. Structural, Optical, Electronic, and Magnetic Properties of Ag-Cu Bimetallic Clusters: A Density Functional Theory Study. *J. Nanopart. Res.* **2018**, *20*, No. 188.
(52) Fernández, E. M.; Soler, J. M.; Garzón, I. L.; Balbás, L. C. Trends in the Structure and Bonding of Noble Metal Clusters. *Phys. Rev. B* **2004**, *70*, No. 165403.
(53) Zhou, Y. H.; Zeng, Z.; Ju, X. The Structural and Electronic Properties of Cu_mAg_n (m+n=6) Clusters. *Microelectron. J.* **2009**, *40*, 832−834.
(54) Ding, L.-P.; Kuang, X.-Y.; Shao, P.; Zhao, Y.-R.; Li, Y.-F. A Comparative Study on Geometries, Stabilities, and Electronic Properties between Bimetallic Ag_nX (X = Au, Cu; n =1−8) and Pure Silver Clusters. *Chin. Phys. B* **2012**, *21*, No. 043601.
(55) Virginia Popa, M. The Electronic Properties of the Silver Clusters in Gas Phase and Water. *Int. J. Comput. Theor. Chem.* **2015**, *3*, 36−57.

https://doi.org/10.1021/acsomega.1c06146
ACS Omega 2022, 7, 2316−2330

(56) Purewal, J. Hydrogen Adsorption by Alkali Metal Graphite Intercalation Compounds. Ph.D. Thesis, California Institute of Technology: Pasadena, CA, 2010.
(57) Aihara, J.-I. Reduced Homo−Lumo Gap as an Index of Kinetic Stability for Polycyclic Aromatic Hydrocarbons. *J. Phys. Chem. A* **1999**, *103*, 7487−7495.
(58) Manolopoulos, D. E.; May, J. C.; Down, S. E. Theoretical Studies of the Fullerenes: C_{34} to C_{70}. *Chem. Phys. Lett.* **1991**, *181*, 105−111.
(59) Ruiz-Morales, Y. Homo−Lumo Gap as an Index of Molecular Size and Structure for Polycyclic Aromatic Hydrocarbons (PAHs) and Asphaltenes: A Theoretical Study. I. *J. Phys. Chem. A* **2002**, *106*, 11283−11308.
(60) Kerpal, C.; Harding, D. J.; Rayner, D. M.; Fielicke, A. Small Platinum Cluster Hydrides in the Gas Phase. *J. Phys. Chem. A* **2013**, *117*, 8230−8237.
(61) Molina, L. M.; Alonso, J. A. Chemical Properties of Small Au Clusters: An Analysis of the Local Site Reactivity. *J. Phys. Chem. C* **2007**, *111*, 6668−6677.
(62) Weinhold, F.; Landis, C. R. *Valency and Bonding: A Natural Bond Orbital Donor−Acceptor Perspective*; Cambridge University Press: Cambridge, U.K., 2005.
(63) Posada-Amarillas, A.; Pacheco-Contreras, R.; Morales-Meza, S.; Sanchez, M.; Schön, J. C. Computational Studies of Stable Hexanuclear $Cu_lAg_mAu_n$ (l+m+n = 6; l, m, n > 0) Clusters. *Int. J. Quantum Chem.* **2016**, *116*, 1006−1015.

https://doi.org/10.1021/acsomega.1c06146
ACS Omega 2022, 7, 2316−2330